Hindawi
Geofluids
Volume 2022, Article ID 7566637, 10 pages
https://doi.org/10.1155/2022/7566637

*Research Article*

# Roof Failure Mechanism of Thin Bedrock Working Faces under Loading and Analysis Based on Microseismic Monitoring Technology

**Wei Miao**,[1,2] **Lin Zhao**,[1] **Shiqi Liu**,[1] **Wenhao Jiang**,[3] **Ermeng Zhang**,[1] **and Jingkai Li**[1]

[1]*School of Energy and Mining, China University of Mining and Technology, Beijing 100083, China*
[2]*Jiaozuo Coal Industry Group, Henan Province, Jiaozuo City 454000, China*
[3]*Zhaoguyi Coal Mine, Henan Province, Xinxiang City 453634, China*

Correspondence should be addressed to Wei Miao; wilson09@126.com and Shiqi Liu; liushiqi0217@qq.com

Received 15 September 2021; Accepted 12 January 2022; Published 16 March 2022

Academic Editor: Zetian Zhang



The resistance transfer coefficient of supports plays an important role in support selection in coal mines, which is the main factor in support crushing accidents. Based on the key layer theory, the formula for calculating the resistance transfer coefficient of supports under the load of a loose layer was deduced. The analysis of four working faces with thick loose layers and the corresponding mining pressure data were used to deduce the load transfer coefficients of the thick loose layers and ultimately illustrate the relationship between thick loose layers and different influencing factors. By using microseismic technology to monitor the process of roof failure in a thin bedrock working face with a thick loose layer during mining, the roof failure characteristics of a large-mining-height working face under the load of a thick loose layer were further verified. The results show that a thicker loose layer and thinner bedrock caused more of the load to transfer to the working face, the roof microseismic events were mainly concentrated in the range of 60 m to 75 m above the coal seam, and the most active events occurred during the square stage (the length of the working face's goaf is equal to its width). The height of the water-conducting fracture zone was analyzed by microseismic data and then verified with theoretical calculations.

## 1. Introduction

There is a widely distributed layer of thick and loose rock overlying a coal seam in eastern and northern China. Often, the roof bedrock is thinner than the height of the water-conducting fracture zone, which is a typical thin bedrock under a thick loose layer, with single key strata. There are great differences between thin bedrock working faces and thick bedrock working faces in terms of stratal movement and overburden failure. According to the many cases of roof caving and roof flooding accidents in China, working faces with thin bedrock and thick loose layers are more likely to experience roof carving, roof water, and sand collapse accidents, which greatly threatens coal mine safety.

Many studies have been conducted to prevent roof pressure disasters in mines with thin bedrock and thick loose layers. A dynamic loading method for achieving a reasonable working resistance of the working face was proposed [1, 2]. Additionally, the law of the random horizontal movement of the thick loose layer under the influence of mining was summarized [3]. The coal seam overburden movement and the control mechanism of thin bedrock coal seams with thick loose layers were studied by various methods [4–6], and the results showed that the stability of the overburden mainly depended on the thickness of the bedrock and loose layers [7, 8]. Engineering practice has shown that, at the working faces, a significant difference in the movement of the thick loose layer and the bedrock was observed [9].

A large number of theoretical studies have focused on the movement and deformation laws of overlying strata and loose strata [10, 11], but the specific influence of loose layer overload on the working face has not been studied and

analyzed; furthermore, the load transfer coefficient of a thin bedrock working face with a thick loose layer has not been deduced. This paper is based on four typical engineering examples collected from different mines of thin bedrock in China. According to the specific influence of the loose layer load on the working face supports under the condition of thin bedrock, the transfer coefficient is obtained, and its influencing factors are analyzed. To monitor the process and the distribution features of working face roof breakage, microseismic monitoring technology was used at a typical thin bedrock working face with a thick loose layer. Based on the distribution features of the microseismic events in the coal seam, the overall height of the caving zone and the water-conducting fracture zone distribution are determined.

## 2. Theoretical Analysis and Governing Equation

*2.1. Analysis of the Loose Layer Load Transfer Effect on the Working Face.* The influence of the loose layer load on the resistance of the working face supports is mainly transmitted through the upper hard roof load. A load on the loose layer is transmitted downward to the upper hard roof and then further transmitted downward to the working face. Therefore, a simple mechanical model is established; that is, in a coal seam with a thick loose layer and thin bedrock structure, the load carried by the working face ($P$) contains the supporting force on the bedrock key layer and the supporting force on the immediate roof:

$$P = P_1 + P_2, \tag{1}$$

where $P_1$ is the supporting force of the broken rock block and $P_2$ is the total supported weight of the immediate roof, false roof, and top coal within the range of the roof control distance.

$$P_2 = \Sigma h \gamma L, \tag{2}$$

where $\Sigma h$ is the thickness of the immediate roof, $\gamma$ is the unit weight of the immediate roof, and $L$ is the hanging arch length of the immediate roof.

In the calculation of the fracture support force of the key strata, the overburden load consists of the load of the loose layer and the load of the key strata in the bedrock, which are the main factors causing the instability of the key strata. Researchers [12, 13] have performed a large number of field measurement studies and concluded that the load transfer effect in the rock strata above the working face does not consider all the weight loaded on the key strata. With transfer coefficients $K_s$ and $K_j$, the formula of the upper load of the key layer is summarized as

$$Q_Z = K_S \sum h_{si}\gamma_{si} + K_J \sum h_{ji}\gamma_{ji}, \tag{3}$$

where $Q_z$ is the weight loaded on the working face, $h_{si}$ is the thickness of the different soil layers, $h_{ji}$ is the thickness of the different rock layers, $\gamma_{si}$ is the unit weight of the different soil layers, and $\gamma_{ji}$ is the unit weight of the different rock layers.

Researchers have established a geomechanical model and deduced that the load transfer coefficient $K_j$ of the upper strata of a thin bedrock working face with a thick loose layer is 0.24~0.30 [14]. Due to the obvious difference in the structure between the upper strata and the loose strata, the transfer coefficient is also greatly different.

Based on the known maximum working resistance $P$ of the support in the thin bedrock working face and the formula above, the transfer coefficient $Ks$ of the load of the loose layer to the working face is deduced:

$$K_S = \frac{P - P_Z + T\ \tan(\phi - \theta) - Q_J - Q_L}{\sum h_{si}\gamma_{si}}, \tag{4}$$

where $Q_J$ is the weight of the bedrock transfer load and $Q_L$ is the load weight of the upper hard roof on the working face support.

*2.2. Analysis of the Load Transfer Coefficient of the Loose Layer in the Working Face.* Table 1 shows the pressure observation data of four typical thick loose layer working faces during mining and the geological data from different mining areas in China; these data are used to deduce the loose layer load transfer coefficient. Because the top coal is not completely released in the top coal caving process, the top coal release rate is calculated to be 60%. According to (4), the load transfer coefficient of the loose layer is obtained by substituting the data of each working face, which are summarized in Table 1. The friction factor used in the process of calculating $\tan(\varphi - \theta)$ is 0.8, the hulking coefficient is 1.3, the mudstone and coal powder sandstone hulking coefficient is 1.50, and the transfer coefficient of the bedrock is set at 0.2. Table 1 shows that the load transfer coefficient of the thick loose layer ranges from 0.017 to 0.087. Other working face data can be analyzed similarly to determine the load transfer coefficient of the loose layer.

According to the derivation results in Table 1, the regression curve and the regression equation between bedrock thickness and transfer coefficient are obtained, which are shown in Figure 1.

Figure 1 shows that with the increase in the thickness of the bedrock in the working faces, the transfer coefficient of the loose layer decreases. The relation between the transfer coefficient and the thickness of bedrock is as follows: when the bedrock is thinner than 40 m, the transfer coefficient decreases slowly; when the bedrock is thicker than 40 m, the transfer coefficient decreases rapidly; and when the bedrock is thicker than 50 m, the transfer coefficient approaches zero. It can be concluded that the thickness of bedrock has an obvious influence on the load transfer coefficient of the loose layer, and the characteristics can be summarized as follows: First, the increase in bedrock thickness is conducive to the formation of a stable bedrock layer structure. The thick bedrock can effectively reduce the subsidence of the rock strata, enhance the stability of the overburden, and efficiently form a stable "voussoir beam" structure, which can bear the load of the overlying loose layer and reduce its transfer coefficient. Second, the increase in bedrock thickness slows the pressure transfer in the working face. As seen from the mining pressure performance data of the working face in Table 1, the increase in bedrock thickness improves the stability of the roof to a certain extent and mitigates the

Table 1: Statistical table of data related to the transfer coefficient of the loose layer in the working face.

| Working face | Thickness of bedrock | Mining height | First weighting distance (m) | Periodic weighting distance (m) | Maximum resistance (kN) | Mining height (m) | Thickness of loose layer (m) | Transfer coefficient |
|---|---|---|---|---|---|---|---|---|
| Longdong Coal Mine 7130 working face | 41.34 | 2.4 | 22 | 12 | 3840 | 270 | 228.66 | 0.017 |
| Longdong Coal Mine 7128 working face | 27.83 | 2.4 | 25 | 15 | 4120 | 230 | 202.17 | 0.073 |
| Zhuxianzhuang Coal Mine 870 working face | 15.9 | 2.2 | 28 | 10 | 2800 | 280 | 264.1 | 0.083 |
| Zhaoguyi Coal Mine 11071 working face | 40.1 | 3.5 | 18.9 | 9.5 | 7980 | 510 | 465.7 | 0.05 |

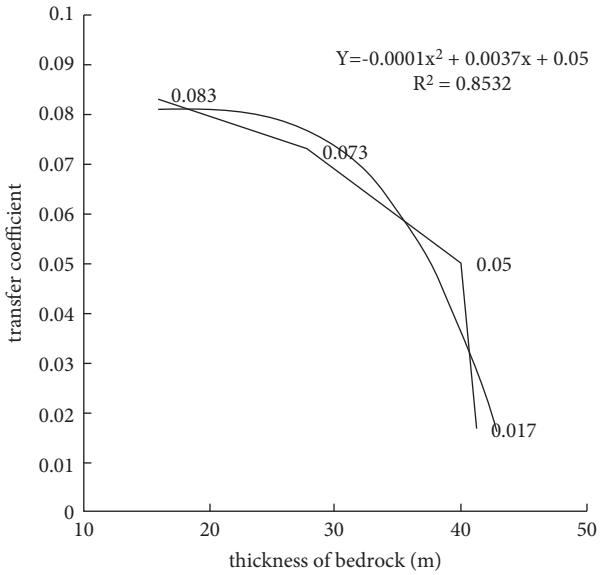


Figure 1: The regression curve of bedrock thickness and transfer coefficient.

damage to the balanced structure of key layers. Third, as the thickness of the bedrock gradually increases, the load transfer coefficient of the loose layer decreases.

In addition, the thickness of the loose layer has a significant influence on the load transfer coefficient of the loose layer. According to the comparison between the 7130 working face of the Longdong Coal Mine and the 11071 working face of the Zhaoguyi Coal Mine in Figure 2, it can be concluded that the 7130 working face of the Longdong Coal Mine and 11071 working face of the Zhaoguyi Coal Mine are similar in terms of bedrock thickness, mining height, first weighting distance, and periodic weighting distance; however, the thickness of the loose layer of the 11071 working face is approximately twice that of the 7130 working face, and the transfer coefficient of the loose layer of the 11071 working face is nearly three times that of the 7130 working face.

It can be summarized that a thicker loose layer will cause a greater load on the bedrock and destroy the balance structure formed by key layers in the bedrock layer, which intensifies the movement of the roof of the working face and makes it difficult to form a stable structure in the bedrock layer; therefore, the transfer coefficient of the loose layer increases.

According to the above analyses, roof collapse and roof water disasters are more likely to occur at working faces with thin bedrock and thick loose layers, and it is necessary to predict the deformation and failure patterns of roof rock in the working face [15, 16]. The methods used to conduct prediction mainly include the empirical formula method, numerical simulation method, borehole observation method, and electric detection method. The accuracy of the empirical formula method and numerical simulation method is lower than that of the field measurement results, while the borehole observation and electrical method are mainly in the form of point observations, and the observation results have certain limitations [17].

## 3. Construction of the Microseismic Monitoring System at the Working Face

*3.1. Principle of Microseismic Monitoring Technology.* The process of surrounding rock stress change is inevitably accompanied by rock mechanics phenomena such as crack expansion and rock mass rupture [18, 19], which lead to microseismic events. Microseismic monitoring technology captures the small vibration signals generated by rock rupture during the formation of water-inrush channels through multiple sets of high-sensitivity geophones arranged in the mining space; the data from the geophones and resulting focal mechanisms are interpreted to locate events in time and space [20] and dynamically analyze the rupture degree and range of the surrounding rock (especially water-resistant coal pillars).

A microseismic monitoring system is mainly composed of working face geophones, underground master stations, ground master controllers, and ground computer terminal modules. The KJ551 microseismic monitoring system was adopted in this study, and its components are shown in Figure 3.

A 20 mm diameter anchor rod is required to install a geophone in the roadway position, and the anchor rod length in the roof needs to be more than 0.5 m. Thus, full-length resin anchorage (more than 0.5 m) was required to ensure stability. To ensure that the anchor rod and the roof were connected firmly, the tray was not installed on the lower side of the anchor rod. The geophone was fixed on the anchor rod to ensure that the geophone installation was in a vertical and downward direction, as shown in Figure 4.

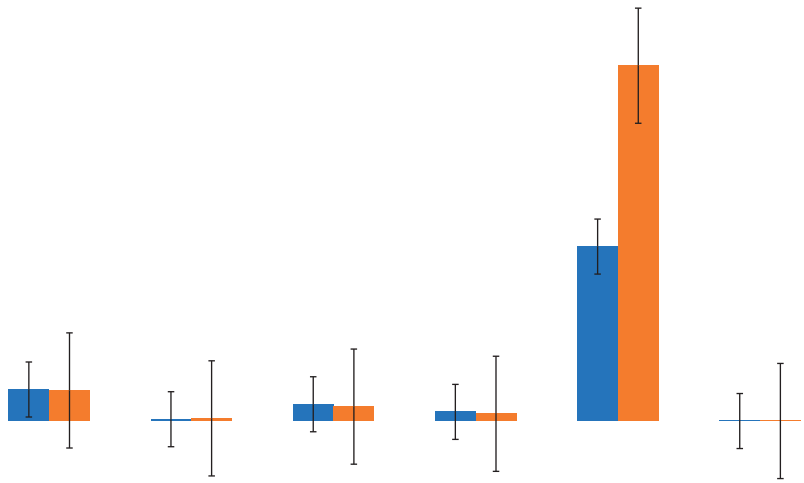

| | Thickness of bedrock (m) | Mining height (m) | First weighting distance (m) | Periodic weighting distance (m) | Thickness of loose layer (m) | Transfer coefficient |
|---|---|---|---|---|---|---|
| 7103 working face | 41.34 | 2.4 | 22 | 12 | 228.66 | 0.017 |
| 11071 working face | 40.1 | 3.5 | 18.9 | 9.5 | 465.7 | 0.05 |

7103 working face
11071 working face

Figure 2: Comparison chart between the 7130 working face and 11071 working face.

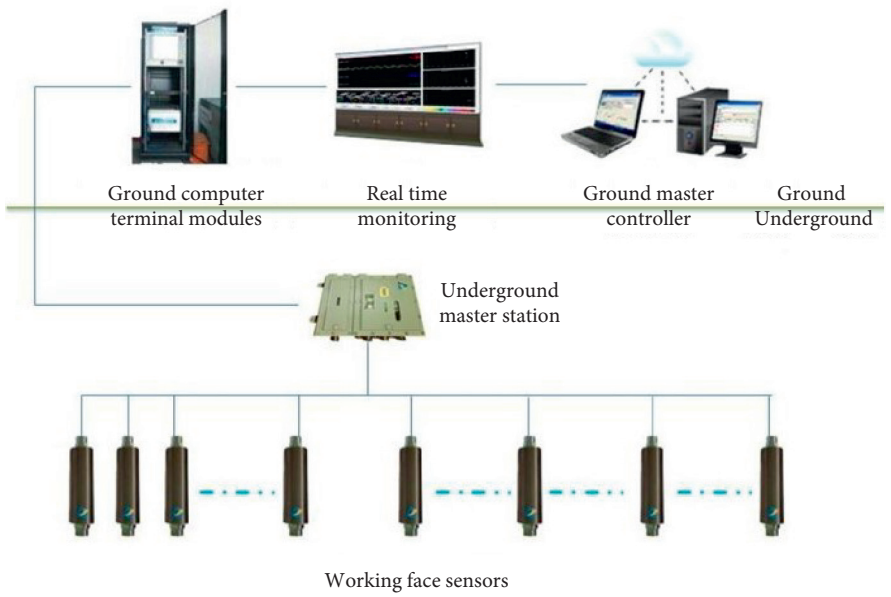


Figure 3: Microseismic monitoring system components.

*3.2. Construction of a Working Face Microseismic System.* A total of 4 roof geophones were installed in the working face, and the first roof geophone was installed 30 m from the open-off cut tunnel in the roadway. The distance between each geophone in the same roadway was 200 m, and the initial layout is shown in Figure 5.

With working face advancement, when the distance between the working face and the geophones became less than 20 m, the geophones were moved outside and maintained at a spacing of 200 m from adjacent geophones. In this way, the geophones remained around the working face until the end of the advancement.

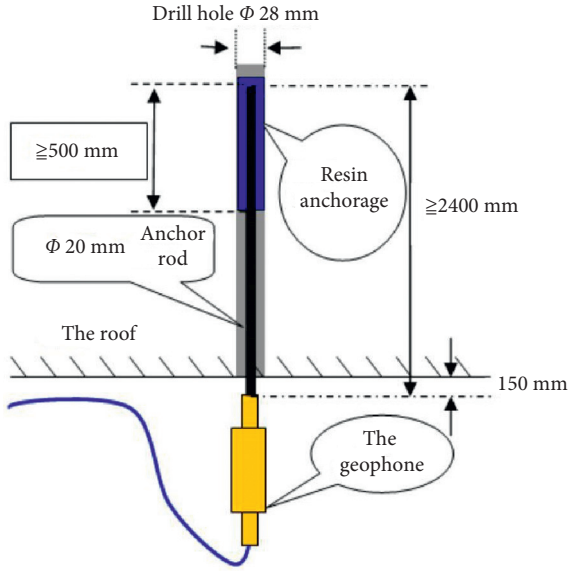


Figure 4: Installation diagram of roof geophone.

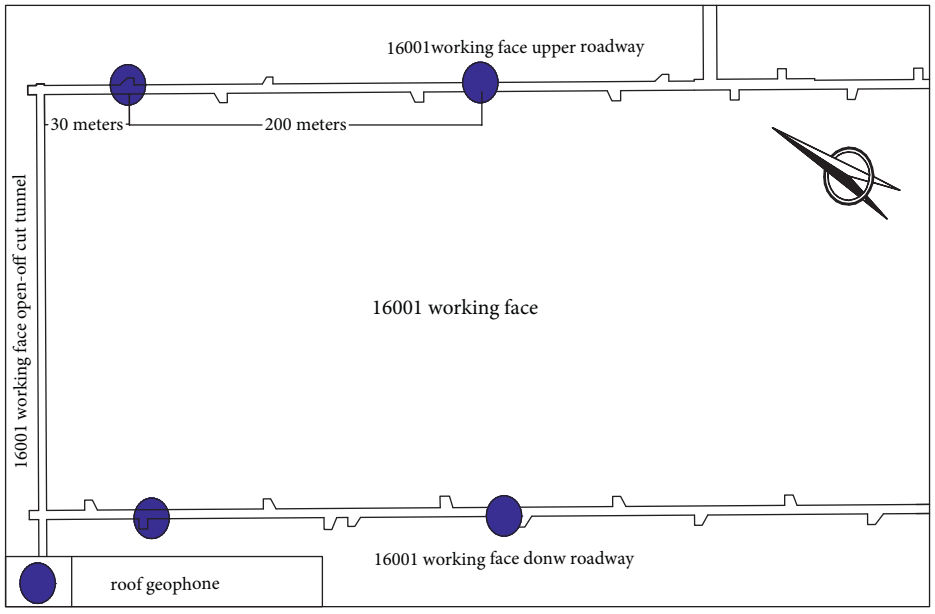


Figure 5: Plan of initial geophone layout.

## 4. Analysis of Roof Failure Characteristics

The microseismic monitoring system was installed in the 16001 working face of the Zhaoguyi Mine to monitor and analyze the roof failure characteristics during working face mining. The mining thickness was 5.8 m to 6.8 m, the roof elevation was −429.9 m to −499.0 m, the working face was 205 m long, the roadways were 901.5 m long on average, with a flat area of 185258.25 $m^2$, the bedrock thickness ranged from 50.0 to 73.7 m, and the loose layer thickness was 410 m. The mining method was large mining height and full thickness mining. Table 2 shows the roof strata of the coal seam.

Monitoring was conducted from January 17, 2018, to January 30, 2019, and a total of 21509 microseismic events with a total energy of 7851083 J and a daily average energy of 23,719 J were analyzed. According to the 16001 working face mining method, microseismic monitoring results, and mine

Table 2: Roof strata of the coal seam.

| Roof type | Lithology | Thickness range (m)<br>Average thickness (m) |
|---|---|---|
| Upper hard roof | Medium sandstone | 2.1–12.3<br>7.2 |
| Immediate roof | Sandy mudstone | 5.3 ~ 21.7<br>13.5 |
| False roof | Mudstone | 0.2 ~ 1.4<br>0.8 |

pressure observation results, the working face mining process can be divided into different mining stages: the initial mining stage, the stage before the square stage, the square stage (the length of the working face's goaf is equal to its width), the stage after the square stage, and the final stage.

*4.1. The Characteristics of the Initial Mining Stage.* The initial mining stage of the 16001 working face was from January 9 to February 21. During this time, the working face was advanced 65.1 m, the daily frequency of microseismic events in this stage was 83 times, and the average daily energy was 15,408 J. From January 19 to January 23, the daily frequency of microseismic events reached 141 times, a 69.8% increase compared to the period before, and the average daily energy released by surrounding rock failure was 26,295 J, a 70.6% increase compared to the period before. According to the microseismic monitoring results, the first weighting of the working face occurred in this period, and the first weighting distance was 27 to 37 m. Figure 6 shows that failures of the surrounding rock were mainly caused by weak energy in the initial mining stage, and the microseismic events in the roof were mostly concentrated within 30 m above the coal seam.

Compared with the working resistance of the supports in the 16001 working face, the characteristics of the initial mining stage were as follows: The pressure detection extension sites in the working face showed that the working face support resistance remained stable before January 21, which was 6341 kN to 8449 kN. The working resistance of the support increased obviously from January 21 to January 23, during which time the working face advanced 33 m to 37 m from the open-off cut tunnel. The working face support resistance increased from 9119 kN to 14223 kN. According to the support resistance monitoring results, the first weighting of the working face occurred on January 22, during which time the working face advanced approximately 35 m from the open-off cut tunnel, and clear increases in pressure and deformation, such as coal wall sliding, occurred frequently.

*4.2. The Characteristics of the Stage before the Square Stage.* In the period of February 21 to May 9, the working face advanced from 65 m to 185 m (measured from the open-off cut tunnel). Compared with the initial mining stage, the average daily frequency of microseismic events was 46 times, the average daily energy was 7,647 J, and the damage to the surrounding rock decreased and maintained stable conditions. It is concluded that in the stage before the square stage, the energy of most microseismic events was less than 500 J, and the events between 100 J and 300 J accounted for nearly 50% of the events, which indicated that the degree of rock failure was low.

Figure 7 shows that the microseismic events that occur in the roof were mainly concentrated within the range of 60 m above the coal seam, and the highest distribution position was approximately 170 m above the coal seam. The density of microseismic events within 60 m to 170 m above the coal seam was far less than that within 60 m above the coal seam. In addition, the microseismic events within 60 m to 170 m above the coal seam were high energy, being scattered and discontinuously distributed, which was consistent with the characteristics of the formation of a high density of rock fractures. Therefore, it was difficult to form a water-conducting fracture zone above 60 m from the coal seam, and the height of the water-conducting fracture zone in the roof was approximately 60 m, which was relatively close to the thickness of bedrock.

*4.3. The Characteristics of the Square Stage.* In the period of May 11 to June 9, the working face advanced from 185 m to 310 m (measured from the open-off cut tunnel), the average daily frequency of the microseismic events was 100 times, and the average daily energy of the microseismic events was 59,616 J. Compared with the previous stages, the energy distribution range of microseismic events increased significantly, and the range of events of 500 J to 1,000 J and the range of events above 1,000 J increased by 11.9%. This period is considered to be the square stage.

Compared with the stage before the square stage, in the square stage, the height of the caving zone of the working face was increased (Figure 8). The microseismic events in the roof were mainly concentrated within 75 m above the coal seam, and the highest distribution position reached approximately 190 m above the coal seam. The density of microseismic events within 75 m to 190 m above the coal seam was far less than that within 75 m above the coal seam, and the microseismic events within 75 m to 190 m above the coal seam were high energy and had a scattered and discontinuous distribution, which can be seen in Figure 8. There were only 8 to 10 energy events over 100,000 J in the upper strata (marked with red circles); therefore, it was challenging to form a water-conducting fracture zone above 75 m. Analysis suggests that the height of the water-conducting fracture zone was approximately 75 m in this stage, which was close to or exceeded the thickness of the bedrock.

*4.4. The Characteristics of the Stage after the Square Stage and the Final Stage.* In the stage after the square stage and the final stage, the average daily energy of the 16001 working face decreased to 11,442 J. The energy of microseismic events between 100 J and 500 J accounted for 70% of the total amount of energy recorded in the two stages, which indicated that the main damage to the surrounding rock occurred near the coal seam, the energy was obviously weaker than that in the square stage, and the movement of the surrounding rock was relatively stable.

Figure 9 shows that the height of the water-conducting fracture zone in the roof of the stage after the square stage was approximately 60 m, which was lower than the height of the water-conducting fracture zone in the square stage.

*4.5. Comparison of Three Stages.* By comparing the distribution of microseismic events from the stage before the square stage to the stage after the square stage, the following characteristics can be found: The energy of microseismic events in the square stage was significantly higher than that in the other two stages (Table 3), and the energy that greater

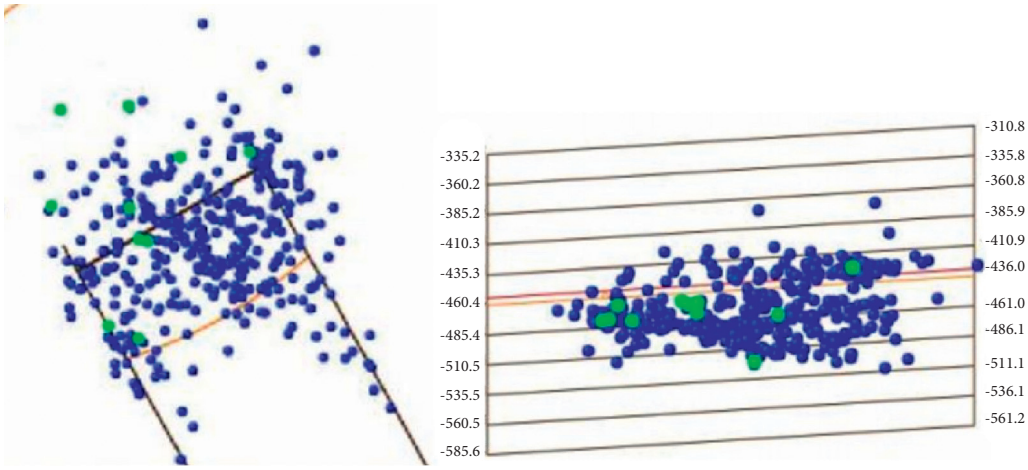


Figure 6: Plan and profile of the 16001 working face microseismic event distribution in the initial mining stage.

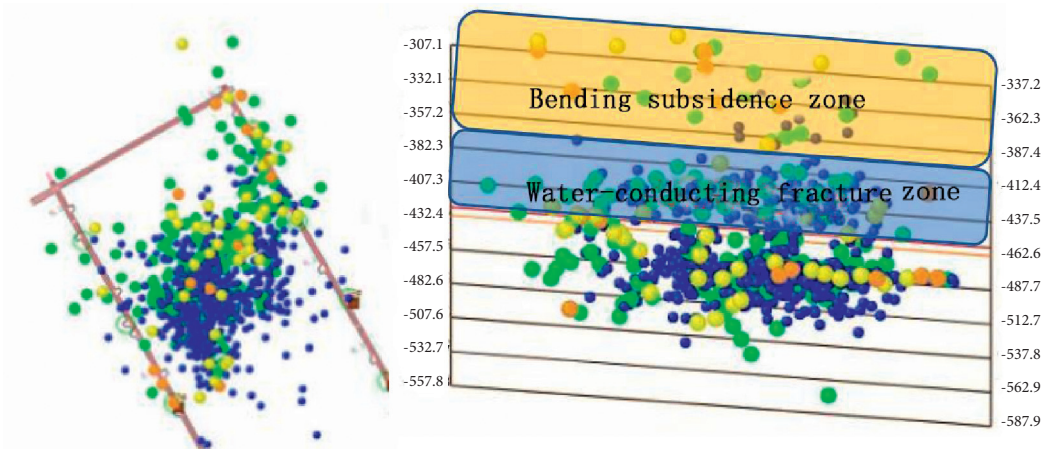


Figure 7: Plan and profile of the 16001 working face microseismic event distribution in the stage before the square stage.

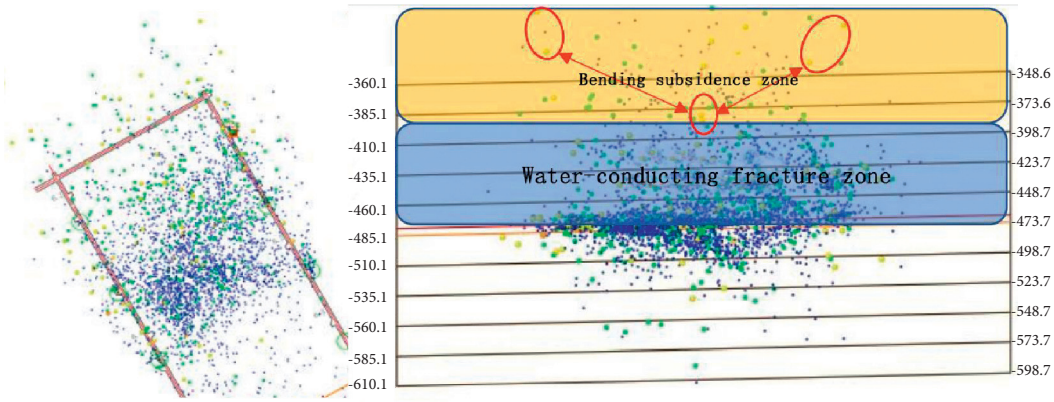


Figure 8: Plan and profile of the 16001 working face microseismic event distribution in the square stage.

than 500 J increased significantly According to the mechanism of structure in the mining length space, when the length of the working face's goaf is equal to its width, the mining supporting pressure reaches the maximum, which is in accord with the microseismic monitoring results. Therefore, the seismic events were mainly distributed in 60 m range above roof in the stage before the square stage; the seismic events were mainly distributed in 75 m range above roof in the square stage; in stage after the square stage, microseismic events were again distributed in 60 m range above roof, which indicated that the square stage was the most active phase of roof rock failure, and the process of water-conducting fracture zone development was recurrent fluctuating.

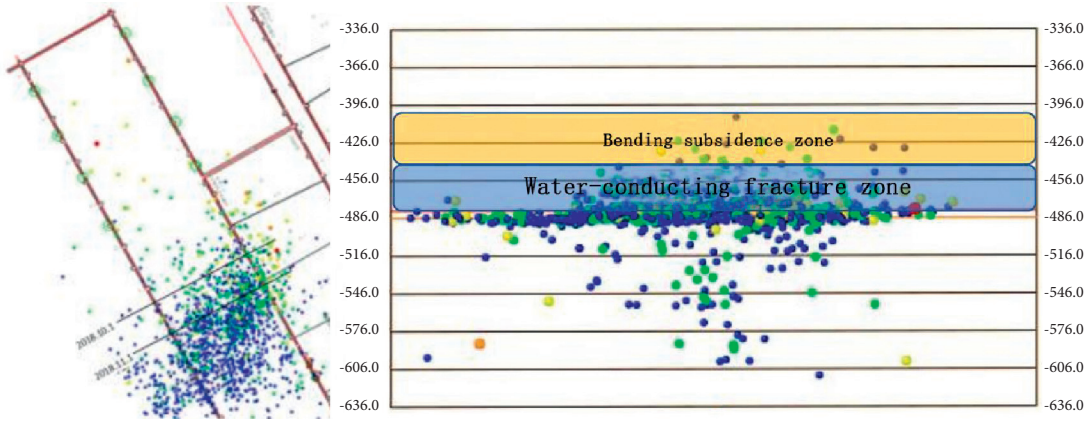


Figure 9: Plan and profile of the 16001 working face microseismic event distribution in the stage after the square stage.

Table 3: The energy percent of three stages.

| Energy (J) | The percent of energy event in stage before the square stage (%) | The percent of energy event in square stage (%) | The percent of energy event in stage after the square stage (%) |
|---|---|---|---|
| 0–100 | 29.8 | 5.1 | 15.0 |
| 101–300 | 49.1 | 35.9 | 42.5 |
| 301–500 | 8.8 | 29.5 | 26.5 |
| 501–1000 | 8.8 | 21.8 | 13.0 |
| > 1000 | 3.5 | 77 | 3.0 |

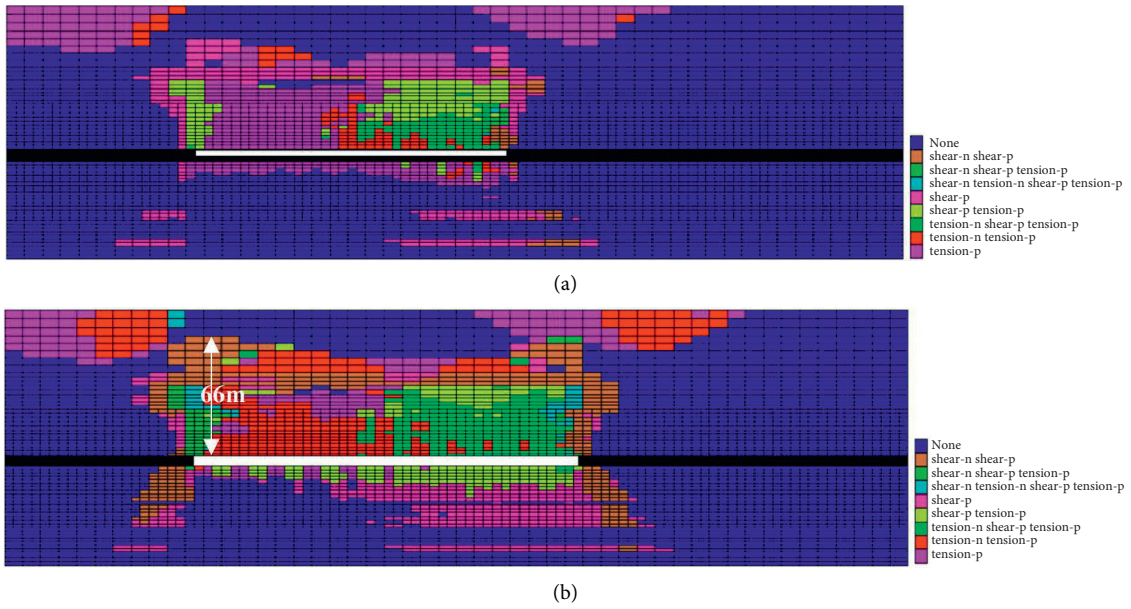


Figure 10: Plastic distribution diagram: (a) the stage before the square stage; (b) the square stage.

### 4.6. Verification

*4.6.1. Verification with Formula Method.* The height of the water-conducting fracture zone can be calculated with the following formula (State Bureau of Coal Industry 2013), and the accuracy has been verified in the Zhaoguer Coal Mine in the same coalfield via field measurements.

$$H_{li} = \frac{100M}{0.26M + 6.88} \pm 11.49, \quad (5)$$

where $M$ is the mining height. The average mining height of the 16011 working face was 5.8 m, and the height of the water-conducting fracture zone of the 16001 working face was 69.15 ± 11.49 m, which is consistent with the results of 60 m to 75 m interpreted with the microseismic method.

*4.6.2. Verification with Numerical Simulation Method.* FLAC3D software is used to conduct numerical simulation calculation of surrounding rock failure rules under the condition of full mining height in the stage before the square stage (advanced 180 m) and the square stage (advanced 220 m) (Figure 10). In the model, the roof height is 80 m above the coal seam.

It can be seen from Figure 10 that the rock mass failure field in the square stage of the working face is significantly larger than that in the stage before the square stage, and the failure range of the plastic zone of the roof reaches the maximum. Shear failure mainly occurs in the rock mass near and in front of the coal wall, indicating that the surrounding rock is subjected to great shear stress after mining. According to the above analysis, the plastic failure zone can be approximately regarded as the water-conducting fracture zone. The figure shows that the maximum height of the plastic failure zone of the roof of 16001 working face is 66 m, which is consistent with the height of the water-conducting fracture zone of the working face of 60 m–75 m monitored by the microseismic monitoring results.

## 5. Summary and Conclusion

(1) The load of a thin bedrock working face with a thick loose layer is composed of the load of the false roof, the immediate roof, the upper hard roof, the bedrock, and the loose layers. The formula of the load transfer coefficient of loose layers is deduced, and based on this formula, the transfer coefficients of the loose layers of four working faces in different areas are calculated, which are 0.017 to 0.087. The regression formula between the thickness of the bedrock and the load transfer coefficient of the loose layer shows that the transfer coefficient approaches zero when the bedrock is thicker than 50 m.

(2) The load transfer coefficient of the loose layer is directly related to the thickness of bedrock in the working face; the thinner the bedrock, the greater the influence of the loose layer on the working face supports. The load transfer coefficient of the loose layer has a certain relationship with the thickness of the loose layer; the thicker the loose layer, the smaller the ratio between the bedrock and the loose layer, and the greater the load transferred to the working face. Microseismic monitoring technology captures the small vibration signals generated by rock rupture during the formation of water-inrush channels through multiple sets of high-sensitivity geophones.

(3) To monitor the process of roof fracture formation and determine the rules of roof weighting in a thin bedrock working face with a thick loose layer, a microseismic monitoring system was applied at the 16001 working face of the Zhaoguyi Coal Mine. Based on the microseismic monitoring results and mine pressure observation results, the working face mining process can be divided into different mining stages: the initial mining stage, the stage before the square stage, the square stage, the stage after the square stage, and the final stage. The monitoring results show that the initial weighting distance of the 16001 working face was approximately 35 m, which is consistent with the pressure data monitored by the working face supports.

(4) The square stage was the most active stage in the mining process, and the height of the water-conducting fracture zone in this stage was approximately 75 m above the coal seam, which is similar to or exceeds the thickness of the bedrock in the roof. The heights of the water-conducting fracture zone in other stages were between 60 m and 70 m, which are basically consistent with the results calculated by the formula. The results indicated that the microseismic monitoring technology applied in the thin bedrock working face with a thick loose layer was successful in monitoring the process of roof failure.

## Data Availability

The data used to support the findings of this study are available from the corresponding author upon request.

## Conflicts of Interest

The authors declare no conflicts of interest.

## Acknowledgments

The authors are grateful to the Zhaoguyi Coal Mine for their partial funding of the in situ experiments and for providing field testing sites and related data. The National Key Basic Research Development Program of China (the Fundamental Research Funds for the Central Universities, 2021YQNY09) is also gratefully acknowledged.

## References

[1] J. Wang, S. Yang, Y. Li, and Z. Wang, "A dynamic method to determine the supports capacity in long wall coal mining," *International Journal of Mining, Reclamation and Environment*, vol. 29, no. 4, pp. 277–288, 2015.

[2] J. Wang and Z. Wang, "Stability of main roof structure during the first weighting in shallow high-intensity mining face with thin bedrock," *Journal of Mining and Safety Engineering*, vol. 31, no. 6, pp. 838–844, 2014.

[3] Y. Xu, S. Liu, Y. Gao, and Q. Zhang, "Study on the internal micro deformation law of thick loose layer," *Coal Science and Technology*, vol. 42, no. 10, pp. 10–13, 2014.

[4] X. Fang, H. Huang, T. Jin, and J. Bo, "Strata behavior of fully-mechanized top coal caving in thin bedrock and thick topsoil," *Journal of Mining & Safety Engineering*, vol. 24, no. 3, pp. 326–330, 2007.

[5] L. Hartley and S. Joyce, "Approaches and algorithms for groundwater flow modeling in support of site investigations and safety assessment of the Forsmark site, Sweden," *Journal of Hydrology*, vol. 129, 2013.

[6] Y. Xu, E. Zhang, Y. Luo, L. Zhao, and K. Yi, "Mechanism of water inrush and controlling techniques for fault-traversing

roadways with floor heave above highly confined aquifers," *Mine Water and the Environment*, vol. 39, pp. 320–330, 2020.

[7] X. Fang, H. Huang, T. Jin, and J. Bo, "Movement rules of overlying strata around long wall mining in thin bedrock with thick surface soil," *Chinese Journal of Rock Mechanics and Engineering*, vol. 27, no. Sup 1, pp. 2700–2706, 2008.

[8] L. Ma, D. Zhang, and G. Sun, "Thick alluvium full-mechanized caving mining with large mining height face roof control mechanism and practice," *Journal of China Coal Society*, vol. 38, no. 2, pp. 199–203, 2013.

[9] J. Zuo, Y. Sun, and M. Qian, "Research on movement mechanism and analogous hyperbola model of overlying strata with thick alluvium," *Journal of China Coal Society*, vol. 42, no. 6, pp. 1372–1379, 2017.

[10] D. Xue, J. Zhou, Y. Liu, and L. Gao, "On the excavation-induced stress drop in damaged coal considering a coupled yield and failure criterion," *International Journal of Coal Science and Technology*, vol. 7, no. 5, pp. 58–67, 2020.

[11] L. Qin, C. Ma, S. Li et al., "Mechanical damage mechanism of frozen coal subjected to liquid nitrogen freezing," *Fuel*, vol. 309, Article ID 122124, 2022.

[12] Q. Huang, P. Zhang, and A. Dong, "Mathematical model of "arch beam" of thick sandy soil layer movement in shallow seam," *Rock and Soil Mechanics*, vol. 30, no. 9, pp. 2722–2726, 2009.

[13] Q. Huang, "Studies on load-transmitting factor of thick sandy soil layer on key roof stratum in shallow seam mining," *Chinese Journal of Geotechnical Engineering*, vol. 27, no. 6, pp. 672–676, 2005.

[14] J. Li, Y. Xu, P. Jiang, and Y. Mou, "Study on load transmission characteristics of overburden rock above coal mining face in thin bedrock of super thick unconsolidated stratum," *Coal Science and Technology*, vol. 45, no. 11, pp. 95–100, 2017.

[15] M. Vanini, M. Corigliano, E. Faccioli et al., "Improving seismic hazard approaches for critical infrastructures: a pilot study in the Po Plain," *Bulletin of Earthquake Engineering*, vol. 16, no. 6, pp. 2529–2564, 2018.

[16] D. Zhou, K. Wu, G. Cheng, and L. Liang, "Mechanism of mining subsidence in coal mining area with thick alluvium soil in China," *Arabian Journal of Geosciences*, vol. 8, no. 4, pp. 1855–1867, 2015.

[17] Y. Liu, Y. Pritam, X. Hu, R. Peng, and T. Bülent, "Effects of electrical anisotropy on long-offset transient electromagnetic data," *Geophysical Journal International*, vol. 222, no. 2, pp. 1074–1089, 2020.

[18] G. Cheng, C. Tang, L. Li, X. Chuai, T. Yang, and L. Wei, "Micro-fracture precursors of water flow channels induced by coal mining: a case study," *Mine Water and the Environment*, vol. 40, 2021.

[19] X. Li, S. Chen, E. Wang, and Z. Li, "Rock burst mechanism in coal rock with structural surface and the microseismic (MS) and electromagnetic radiation (EMR) response," *Engineering Failure Analysis*, vol. 124, 2021.

[20] C. Zhang, G. Jin, C. Liu et al., "Prediction of rockbursts in a typical island working face of a coal mine through microseismic monitoring technology," *Tunnelling and Underground Space Technology*, vol. 113, 2021.